ACCOUNTS of chemical research

Article

pubs.acs.org/accounts

Emergent Properties of Dense DNA Phases toward Artificial Biosystems on a Surface

Dan Bracha, Eyal Karzbrun, Shirley S. Daube, and Roy H. Bar-Ziv*

Department of Materials and Interfaces Weizmann Institute of Science, Rehovot 76100, Israel

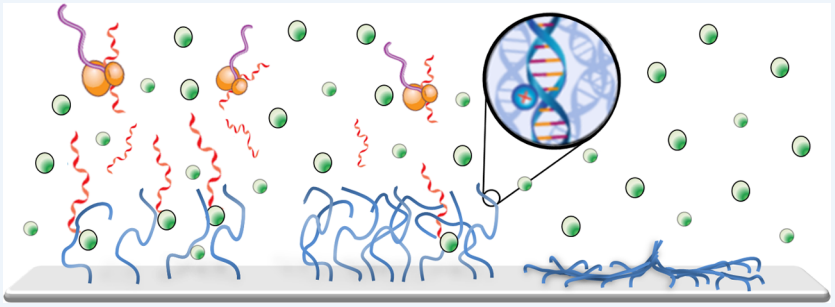

CONSPECTUS: The expression of genes in a cell in response to external signals or internal programs occurs within an environment that is compartmentalized and dense. Reconstituting gene expression in man-made systems is relevant for the basic understanding of gene regulation, as well as for the development of applications in bio- and nanotechnology.

DNA polymer brushes assembled on a surface emulate a dense cellular environment. In a regime of significant chain overlap, the highly charged nature of DNA, its entropic degrees of freedom, and its interaction with transcription/translation machinery lead to emergent collective biophysical and biochemical properties, which are summarized in this Account.

First, we describe a single-step photolithographic biochip on which biomolecules can be immobilized. Then, we present the assembly of localized DNA brushes, a few kilo-base pairs long, with spatially varying density, reaching a DNA concentration of $\sim 10^7$ base pairs/μm^3, which is comparable to the value in *E. coli*.

We then summarize the response of brush height to changes in density and mono- and divalent ionic strength. The balance between entropic elasticity and swelling forces leads to a rich phase behavior. At no added salt, polymers are completely stretched due to the osmotic pressure of ions, and at high salt they assume a relaxed coil conformation. Midrange, the brush height scales with ratio of density and ionic strength to the third power, in agreement with the general theory of polyelectrolyte brushes. In response to trivalent cations, DNA brushes collapse into macroscopic dendritic condensates with hysteresis, coexistence, and a hierarchy of condensation with brush density.

We next present an investigation of RNA transcription in the DNA brush. In general, the brush density entropically excludes macromolecules, depleting RNA polymerase concentration in the brush compared to the bulk, therefore reducing transcription rate. The orientation of transcription promoters with respect to the surface also affects the rate with a lower value for outward compared to inward transcription, likely due to local changes of RNA polymerase concentrations. We hypothesize that equalizing the macromolecular osmotic pressure between bulk and brush with the addition of inert macromolecules would overcome the entropic exclusion of DNA associated proteins, and lead to enhanced biochemical activity.

Finally, we present protein synthesis cascades in DNA brushes patterned at close proximity, as a step toward biochemical signaling between brushes. Examining the synthesis of proteins polymerizing into crystalline tubes suggests that on-chip molecular traps serve as nucleation sites for protein assembly, thereby opening possibilities for reconstituting nanoscale protein assembly pathways.

INTRODUCTION AND MOTIVATION: DNA BRUSHES AS SYNTHETIC CELLULAR ENVIRONMENTS

Cellular microenvironments where gene expression takes place, such as the nucleus of eukaryotic cell or the bacterium nucleoid, are crowded in nucleic acids, proteins, and multivalent ions.[1] To give a sense of scale, the *E. coli* genome is 4.6×10^6 base pairs (bp) long, coding for $\sim 4 \times 10^3$ proteins in a volume of $\sim 0.7\ \mu m^3$, which amounts to ~10 mg/mL DNA, in an overall macromolecular concentration of approximately 300 mg/mL.[2] Such values are significantly denser than reactions reconstituted in vitro. For example, protein synthesis from a plasmid is typically done at a concentration of 10^{-2} mg/mL in ~20 mg/mL cell extract. Thus, in vitro gene expression in a bulk reaction differs by orders of magnitude from cellular conditions.

Reconstituting gene expression in spatially controlled synthetic systems can help us understand the interplay between

Special Issue: Nucleic Acid Nanotechnology

Received: March 31, 2014
Published: May 23, 2014

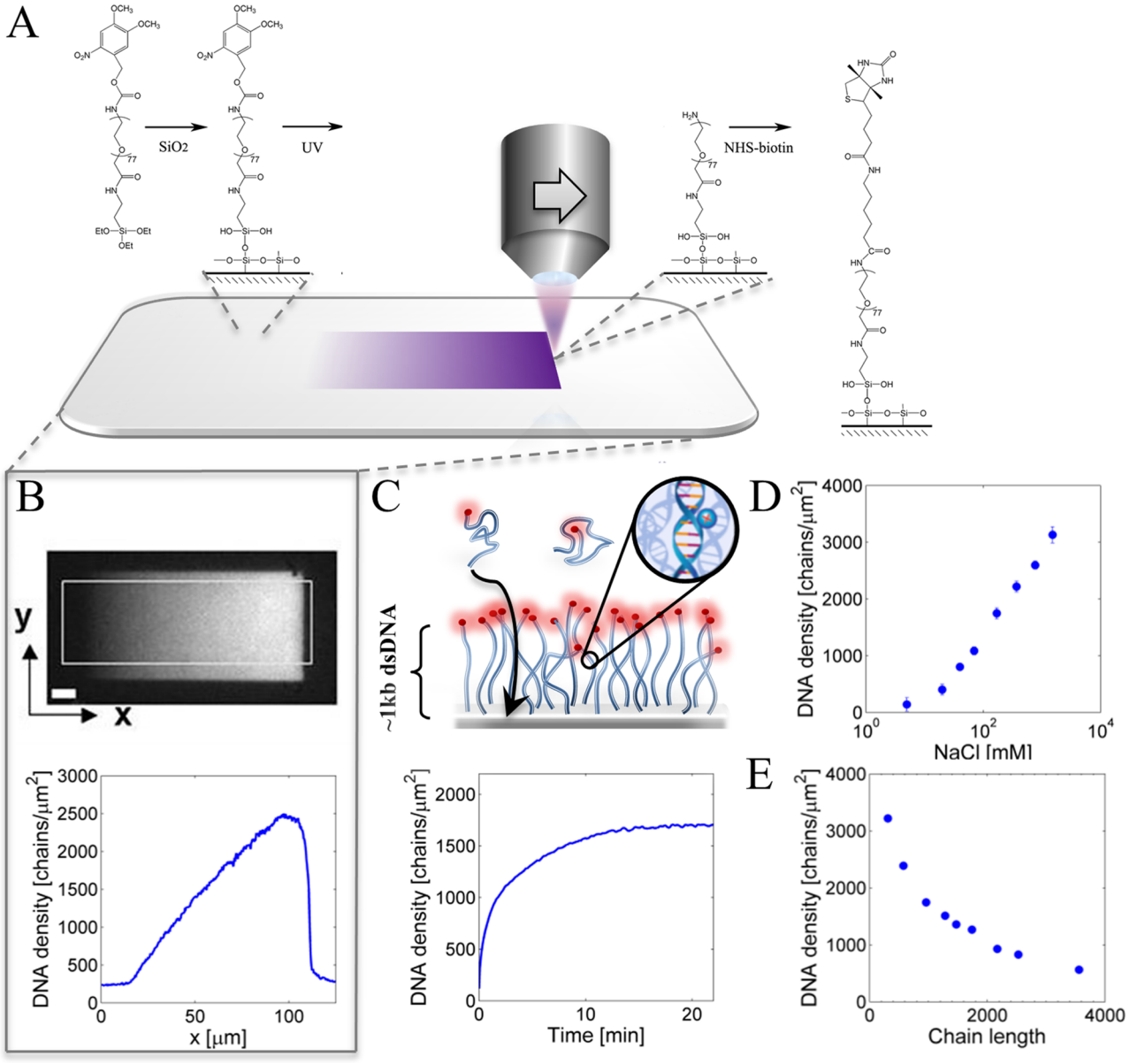

Figure 1. DNA brush patterning and assembly on a biochip. (A) A self-assembled, photosensitive monolayer based on PEG is formed on a glass surface. Exposing the surface to UV deprotects primary amines that are coupled to biotin moieties by NHS chemistry for subsequent binding of streptavidin conjugated biomolecules. Reproduced with permission from ref 42. Copyright 2007 WILEY VCH. (B) Immobilized DNA chains (1 kbp, fluorescently end labeled) along a density gradient of biotin binding sites, yielding a DNA brush with linearly increasing density up to ~2500 chain/μm^2 (scale bar is 5 μm). Adapted from ref 45. (C) Kinetics of brush assembly at 150 mM NaCl revealed by TIRF measurement. Saturation is reached although most binding sites remain unoccupied. (D) Brush density increases with salt concentration and (E) decreases with chain length.

the organization of matter and biomolecular information processing in crowded environments. For example, a hybrid system capable of exhibiting emergent spatial gene expression patterns from surface bound circuits, could serve as a model system for processes taking place during early embryo development.[3,4] Localized cell-free expression of multicomponent assemblies could also address the origin of high-fidelity in biological nanomachines, for example, the biogenesis of a ribosome[5] or T4 bacteriophage assembly line.[6] Thus, developing spatially controlled gene expression platforms at the cellular scale would contribute to the growing effort toward in vitro programmable protein and nucleic-acid systems. Recent examples include gene expression and transcriptional circuits in bulk solution or gels,[7−14] encapsulation of expression in vesicle bioreactors,[15−18] semipermeable microcapsules[19] and coacervates,[20] networks in droplet compartments,[21] DNA-based computational circuits,[22−24] neural networks,[25] in vitro integration of multisubunits enzymes and ribosomes,[26−28] cell-free bacteriophage protein synthesis and assembly,[29−31] and memory devices;[32] yet a comprehensive review[33−41] is beyond the scope here.

To this end, we have been studying DNA polymer brushes as spatially defined cell-free gene expression platforms in contact with a cytosol-like reservoir. These brushes are assembled with interchain distances of the order of the dimensions of an RNA polymerase or a ribosome, where interactions lead to emergent biophysical and biochemical collective behavior. In this Account, we give an overview of our work on DNA brushes, describing first the immobilization on a biochip[42,43] with new data on the kinetics of assembly, followed by a physical study

dx.doi.org/10.1021/ar5001428 | Acc. Chem. Res. 2014, 47, 1912−1921

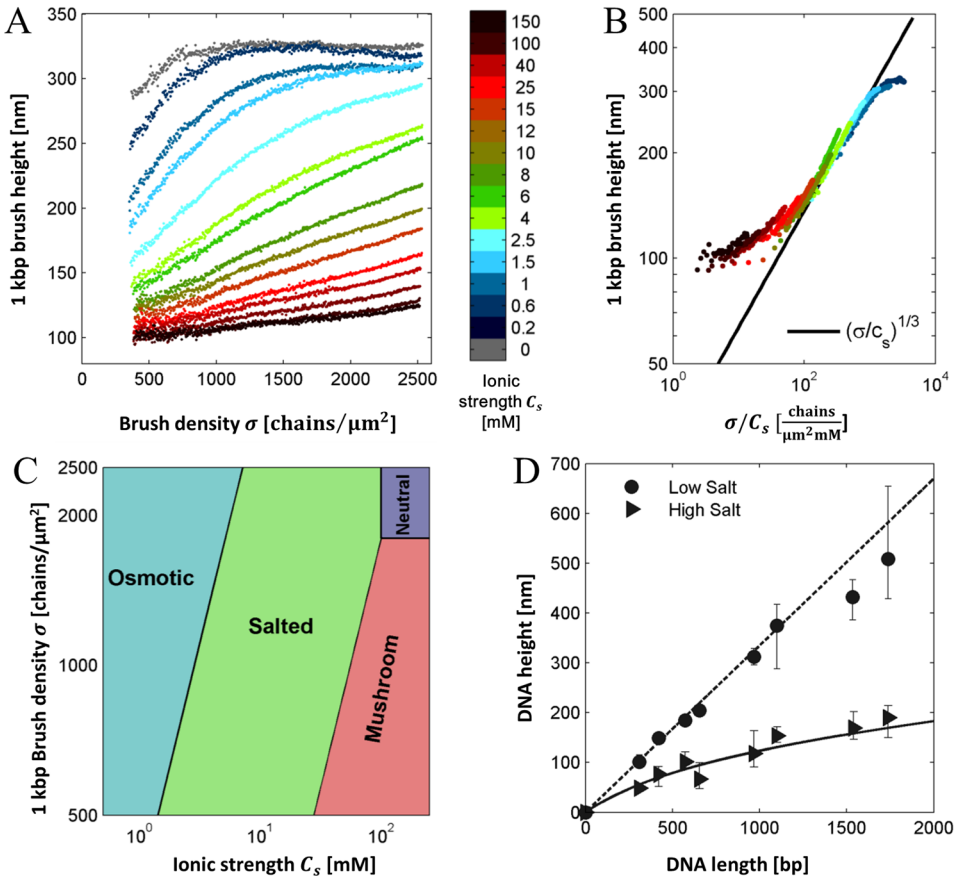

Figure 2. Entropy-driven collective conformations of a DNA brush. (A) Height measurement of a 968 bp DNA brush as a function of DNA surface density and NaCl ionic strength (color coded). (B). Data collapse of brush height h as a function of DNA density to ionic strength ratio σ/c_s with power-law scaling $h \propto (\sigma/c_s)^{1/3}$ (solid line). (C) Phase diagram of the osmotic, salted, quasi-neutral, and mushroom brush regimes. (D) Brush height as a function of DNA contour length at low salt (circles, 0.1 mM NaCl) and high salt (triangles, 250 mM NaCl). Fits correspond to $h \approx N_p l_p$ (dashed line) and wormlike chain model (solid line). Reproduced from ref 45.

on the phase behavior in response to DNA density and ionic strength.[44−46] We then review our biochemical investigation of RNA and protein biosynthesis from the brush[47,48] with new direct measurements of the effect of DNA density on RNA polymerase localization in the brush. Finally, we summarize our efforts to spatially pattern protein expression cascades and protein traps.[31,42,49]

DNA BRUSH ASSEMBLY ON A PHOTOCHEMICAL BIOCOMPATIBLE CHIP

Our lab has developed a biochip for precise immobilization of a variety of biomolecules at high spatial resolution, while maintaining essential biochemical activity, such as transcription from DNA templates. The biochip is based on a bifunctional polyethylene glycol (PEG) with a photolabile group protecting a reactive amine at one end and an organosilane at the other end (Figure 1A).[42] This chimera molecule forms a self-assembled monolayer on any silicon dioxide surface, including a 10 nm thin glass film used as an electron microscopy substrate.[31] The monolayer has a spacing of less than 2 nm between molecules and an extension of ∼10 nm from the solid surface when hydrated, which ensures minimal nonspecific adsorption of biomolecules. The caged amines are deprotected by 365 nm UV light with complete uncaging at an energy flux of ∼2500 J/cm^2.[42] UV exposure time and intensity are controlled to create patterns of spatially varying density of amines. *N*-Hydroxysuccinimide (NHS) chemistry is then used for directly linking the amines to biotin, which in turn bind a variety of streptavidin conjugated biomolecules such as DNA (Figure 1A, B).[42]

The kinetics of double stranded DNA brush assembly was monitored using fluorescence labeling at the DNA surface-distal end. Initially dictated by diffusion of DNA polymers from bulk to surface, brush density saturates when further chain penetration is inhibited at high brush density, despite a large fraction of unbound sites remaining on the surface (Figure 1C). Values of DNA density were determined both by using radioactively labeled bases and by UV absorption, offering means to convert arbitrary fluorescent units.[42,47] What sets the DNA brush density? The maximal density increases with ionic strength (Figure 1D) and decreases with DNA length (Figure 1E). Typically, for a 1 kilo-base pairs (kbp) DNA, a 10-fold increase in monovalent salt (above a threshold of 10 mM) increases the density by a factor of 2.5. At 150 mM salt, the brush density drops with DNA length from 3000 to 600 chains/μm^2 for 0.3 and 3.6 kbp chains, respectively. A density of 2000 chains/μm^2 corresponds to a mean distance of ∼20 nm between chains, at which DNA−DNA interactions play a role.

dx.doi.org/10.1021/ar5001428 | *Acc. Chem. Res.* 2014, 47, 1912−1921

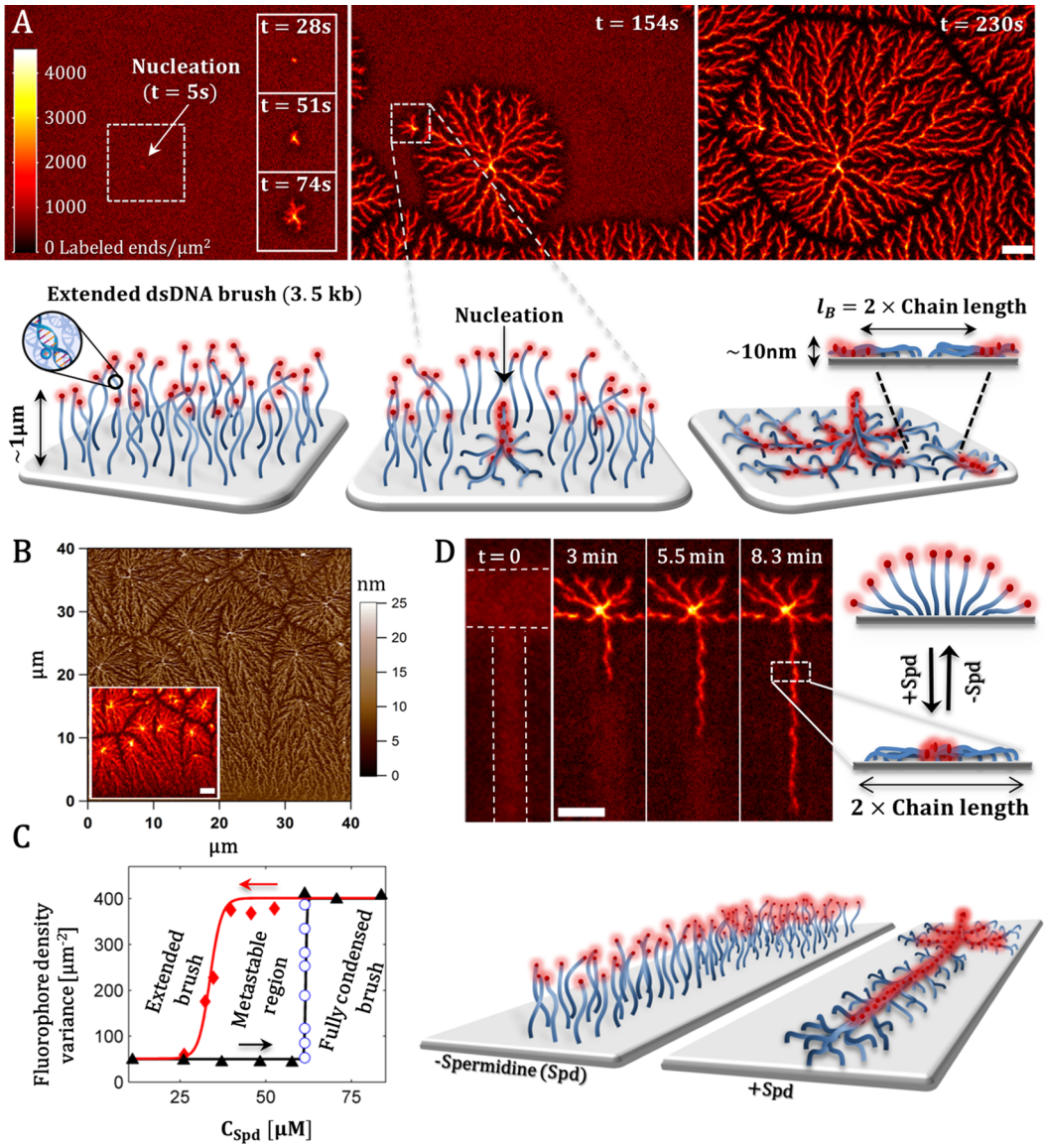

Figure 3. Dendritic assemblies of condensed DNA brush induced by spermidine^{3+}. (A) Fluorescence images with their schematic illustration of a uniform 3.5 kbp osmotic brush undergoing condensation by nucleation and growth at t = 5, 28, 51, 74, 154, and 230 s from the addition of Spd. (B) Wet AFM topography of DNA brush after termination of condensation indicates a height decrease by 2 orders of magnitude compared to an extended uncondensed brush (~1 μm). (C) Reversibility, metastability, and hysteresis are observed in a condensation−decondensation cycle (black triangles and red diamonds, respectively) in response to changing Spd concentration. Open blue circles represent the time-dependent variance of the fluorescence intensity distribution during condensation. (D) Brush collapse into a single nanowire-shaped condensate accomplished by assembling a DNA brush along a patterned line narrower than twice the DNA contour length next to a denser rectangular brush acting as a nucleation-prone site. Scale bars are 5 μm. Color code indicates local fluorophore density of the DNA labeled ends. Reproduced from ref 46.

BRUSH HEIGHT IS DETERMINED BY IONIC STRENGTH AND DNA DENSITY

As for any polyelectrolyte brush, the DNA brush extends away from the surface to a height that is determined by equilibrium between the entropic elasticity of the DNA polymers and swelling forces, such as electrostatic repulsion and excluded volume interactions.[50−53] To explore the DNA brush physics and to quantify the underlying forces, the average brush height was measured as a function of density and bulk ionic-strength (Figure 2).[45] An ~1 kbp DNA brush pattern (100 × 50 μm^2) was assembled with a density gradient $\sigma(x)$ ranging from 400 to 2500 chains/μm^2 along the x-axis (Figure 1B).[44,45] The brush height $h(x)$ was measured using total internal reflection fluorescence (TIRF) of DNA polymer ends, with emission intensity $\sigma(x)\, e^{-h(x)/\xi}$, and an evanescent decay length $\xi \sim 120$ nm (Figure 2A). The local DNA density $\sigma(x)$ was determined by epifluorescence imaging of the end-labeled DNA.

A threefold change in height was measured, from a minimal value of ~100 nm at high monovalent salt ($c_s \geq 100$ mM) to complete extension of ~320 nm at no added salt, independently of brush density. Midrange ($0.2 \leq c_s < 100$ mM), the brush stretched out gradually with increase in density or decrease in ionic strength. Data collapse of brush height as a function of density to ionic strength ratio (σ/c_s) was obtained for density $\sigma <$ ~2000 chains/μm^2 (Figure 2B). At $\sigma/c_s \sim$ 100−1000 (chains · μm^{-2} · mM^{-1}), a power-law scaling regime with $h \propto (\sigma/c_s)^{1/3}$ was observed. Similar scaling was also observed in the presence of divalent magnesium chloride.[45]

dx.doi.org/10.1021/ar5001428 | Acc. Chem. Res. 2014, 47, 1912−1921

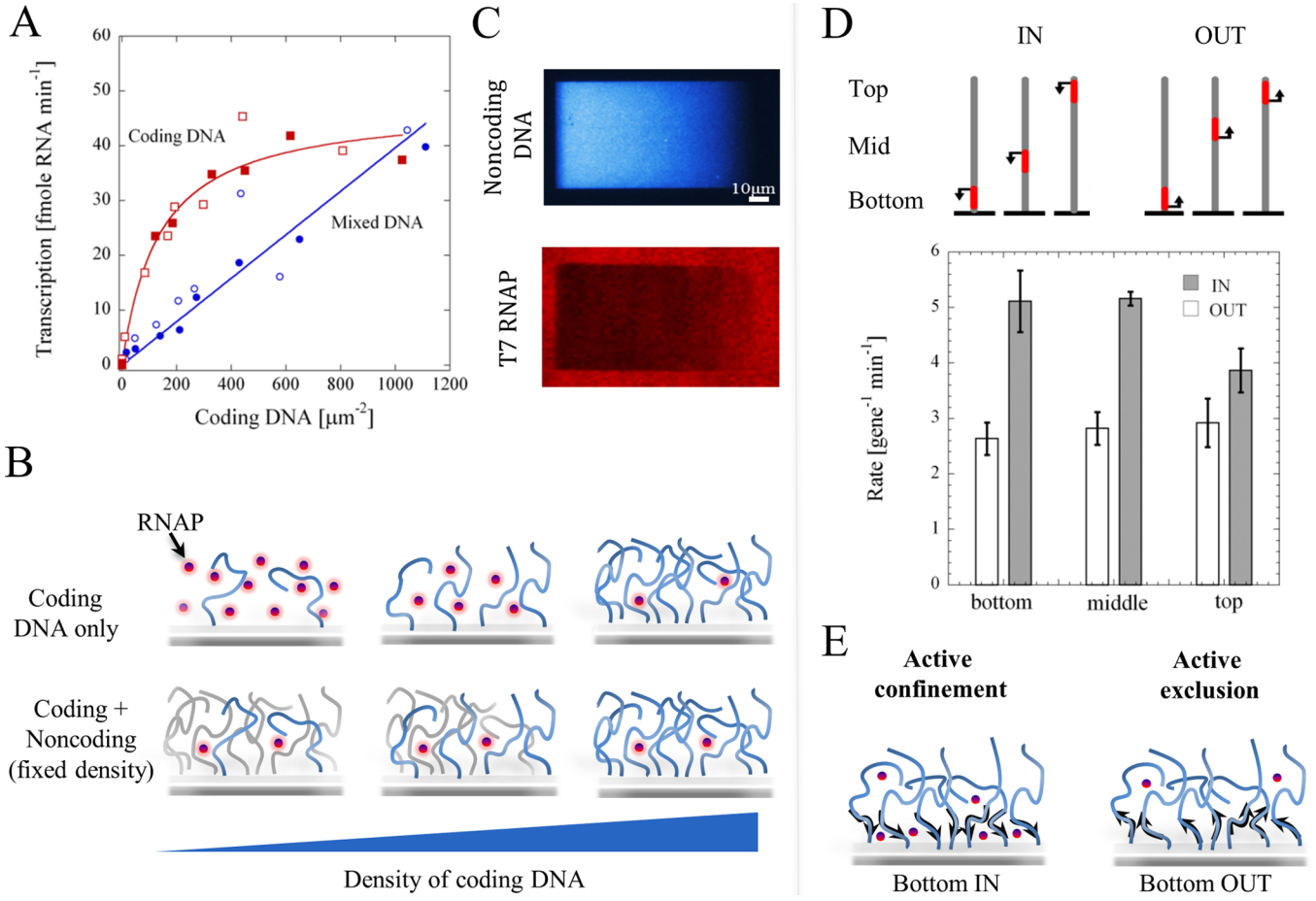

Figure 4. Passive and active partitioning of T7 RNA polymerase. (A) Transcription rate as a function of coding DNA copy-number at increasing surface density (red rectangles) or when fixed to high density via the addition of noncoding DNA (blue circles). Reproduced from ref 48. (B) Scenario for the reduction in transcription efficiency with density due to RNAP (red circles) depletion. Brushes are assembled from only coding (blue) chains or mixed coding and noncoding (gray) chains. (C) Direct TIRF measurement of fluorescently labeled RNAP (red) within a density gradient of noncoding DNA (blue), supporting the scenario presented in (B). (D) Transcription rates are higher for genes oriented toward the surface (IN) relatively to genes oriented toward (OUT) the reservoir. Reproduced from ref 48. (E) Scenario for active RNAP partitioning depicting the effect of gene directionality on RNAP concentration within the brush. Inward transcription enriches the RNAP pool, while outward transcription acts with the passive exclusion further decreasing the internal concentration. Colors as in (B).

The brush height scaling with density and ionic strength was previously predicted in a general theory of polyelectrolyte brushes.[50] The polymer counterions in a highly charged brush were theoretically shown to be confined within the brush volume due to electrostatic interactions. Accordingly, the counterion concentration in a DNA brush of ~1000 chains/μm^2 amounts to $c_0 \sim 1$ mM at zero ionic strength of the immersing solution, $c_s = 0$.[45] The ion concentration imbalance between the brush phase and the immersing solution creates an osmotic pressure that drives the extension of the brush. In the presence of added salt, the ions' osmotic pressure $\Pi_{ions} \propto (\sigma^2 N_p^2)/(c_s h^2)$ increases with the DNA density σ and the number of persistence lengths N_p, and decreases with the brush height h and ionic strength.[50]

The osmotic pressure of ions is balanced by the entropy of the DNA polymer that resists stretching. The loss of configurational entropy due to DNA extension results in a contracting force that is linear in the brush height $F_{entropy} \propto (\sigma/N_p)h$ similarly to the force exerted by a stretched spring. The equilibrium height $h_s \propto N_p l_p (\sigma/c_s)^{1/3}$ is linear in the contour length $N_p l_p$ where $l_p \approx 50$ nm is the DNA persistence length. The predicted power-law scaling of height with the ratio of density and ionic strength was measured in a wide range of parameters ($100 < \sigma/c_s < 1000$ [chains·μm^{-2}·mM^{-1}], Figure 2B). This behavior, in which DNA responds to changes in the ionic strength, was previously defined as the *salted brush* regime.[50]

Three additional scaling regimes were identified: mushroom, quasi-neutral, and osmotic (Figure 2C). (i) Mushroom regime: At high ionic strength and at low brush density ($\sigma/c_s < 100$ [chains · μm^{-2} · mM^{-1}], Figure 2B), the osmotic pressure becomes negligible and the brush shrinks to a minimal height that is independent of density. The brush height as a function of polymer contour length fits well with the end-to-end distance of a semiflexible polymer in solution following the wormlike chain model, $R_{WLC}^2 = 2N_p l_p^2 - 2l_p^2(1 - e^{-N_p})$ (Figure 2D).[54,55] (ii) Quasi-neutral brush: At high ionic strength and a very high density ($c_s > 100$ mM, $\sigma > 2000$ chains/μm^2, Figure 2A), we observed the brush height scaling with density, $h_N \propto N_p l_p \sigma^{1/3}$. This scaling is expected for a neutral brush with excluded volume interactions.[56] (iii) Osmotic brush: At low ionic strength, $c_s < c_0$, and a high density ($\sigma/C_s > 1000$ [chains · μm^{-2} ·mM^{-1}], the osmotic pressure of the confined counterions is large enough to induce maximal extension of the brush.

dx.doi.org/10.1021/ar5001428 | Acc. Chem. Res. 2014, 47, 1912−1921

Under this regime, the brush height scaled linearly with the polymer contour length, $h_0 \approx N_p l_p$, which is the manifestation of a polymer brush (Figure 2D).

CONDENSATION OF DNA BRUSHES INTO COLLAPSED DENDRITIC DOMAINS

In contrast to the gradual conformational effect of mono- and divalent ions on relaxed DNA in solution, multivalent cations, such as spermidine^{3+} (Spd), have been shown to induce a sharp phase transition into a compacted state of locally aligned DNA segments separated by distances of ~3 nm.[57−59] This process, known as DNA condensation, plays a fundamental role in DNA packaging, genome protection, and gene-expression regulation in vivo.[60,61] When subjected to a critical Spd concentration, DNA brushes collapsed from an extended conformation (e.g., ~1.1 μm height for 3.5 kb chains) to macroscopic condensed structures that are no more than 25 nm in height (Figure 3B).[46] The transition began with the local gathering of chains into focal nucleation centers that emerged randomly within a homogeneous brush (Figure 3A). Chains located at the nuclei-brush interface then began collapsing toward the nucleation center, thus forming a radially growing condensate with continuously branching ~50 nm wide fibers. Sharp boundaries of oppositely collapsed chains were formed at the interface between growing domains (Figure 3B). The resulting dendritic structure likely maximizes DNA−DNA contact area under the constraints of chain immobilization and DNA bending rigidity, similarly to DNA toroid formation in dilute solution.[62]

The direct visualization of DNA condensation in brushes provided means to mechanistically investigate the process. We found that, beyond a critical brush density, a further increase in density significantly shortened the lag time for nucleation, and accelerated the lateral growth rate.[46] The extended conformation was found to be a prerequisite for dendritic growth with chains maintaining their extended state during collapse. Condensation was reversible and hysteretic with Spd concentration (Figure 3C) allowing trapping the brush in a metastable state of coexistence between condensed and noncondensed DNA phases, reminiscent of genome organization in living cells.[63] Understanding the mechanism of condensation combined with surface patterning of DNA density was used to demonstrate guided growth from a focal nucleation of 50 nm wide, 50 μm long nanowire of a condensed DNA brush (Figure 3D).[46]

MODULATION OF RNA TRANSCRIPTION BY DNA BRUSH PROPERTIES

DNA brushes provide a unique platform to study the effect of DNA segregation, local density and organization on gene expression. To that end, we measured the transcription rate of T7 RNA polymerase (RNAP) from RNA-encoding brushes as a function of DNA density and promoter orientation relative to the surface.[48] As a first step, discrete brushes with increased density were assembled from coding DNA with promoters directing transcription into the surface. The resulting transcription level increased at a decelerating rate with brush density, reaching a saturating value (Figure 4A, B). To elucidate the source of inhibition at high DNA densities, we decoupled the number of coding DNA from the DNA density by adding noncoding DNA to each of the brushes to supplement it such that the overall DNA density was kept constant at the highest value. At this high DNA density, transcription rate was now linearly dependent solely on the amount of coding DNA within the brush. Interestingly, for the same amount of coding DNA on the surface, transcription rates were always lower than those measured in coding-only, hence more dilute, DNA brushes (Figure 4A, B).

Ruling out ion depletion or nonspecific binding of RNAP to noncoding sequences as the source of transcription inhibition, we hypothesized that transcription inhibition with density was due to RNAP exclusion from the dense DNA brush.[48] This hypothesis is supported by a new direct measurement of a gradual depletion of labeled RNAP from a continuous gradient of noncoding DNA using TIRF microscopy (Figure 4C). We speculate that despite the electrostatic attraction of RNAP to DNA,[64] it is entropy that drives the polymerases out from the crowded microenvironment of the brush and into the dilute reservoir. Namely, high DNA density passively partitions RNAP (Figure 4B), thus dictating the rate of transcription.

Unique to DNA brushes, transcription levels could be modulated by DNA orientation. This has been shown by assembling brushes of similar density, each having its coding sequences (280 bp) facing either the surface (IN) or the reservoir (OUT) and positioned differently along the DNA (bottom, middle, or top, Figure 4D). Despite an overall lower transcription rates in the brush relative to bulk solution, we found that the direction of the coding sequence affected the rate, yielding more than a 2-fold higher rate for IN than OUT configurations. When a much longer transcription unit of the 1.6 kbp long luciferase gene was coded in a 2.1 kbp brush, more than 5-fold increase in transcription rate was observed for IN over OUT configuration.[47] Thus, the directionality of RNA synthesis seems to partition RNAP in an active mechanism (Figure 4E): An IN orientation creates a gradient of RNAP into the brush thus opposing the macromolecular exclusion, while an OUT orientation further reduces the internal concentration of RNAP by driving it out of the brush.

Overall, we observed macromolecular partitioning between the brush and the surrounding reservoir that is dictated passively by DNA local density and actively by the directionality of RNA synthesis. Such partitioning is obtained in cells either by membranes that create a permeable barrier defining segregated compartments or in membraneless pseudocompartments such as the bacterial nucleoid, where the chemical nature of the microenvironment dictates heterogeneous macromolecules distribution.[65,66] Accordingly, DNA brushes create a compartmentalized environment by breaking the symmetry of the reaction, with brush length, density, and promoter orientation creating an effective boundary and macromolecular composition differences. DNA brushes thus provide a synthetic platform to probe effects of gene clustering and spatial organization on gene expression, which have been shown to play a role in vivo yet are difficult to be systematically studied outside a living organism.[67−71]

CELL-FREE SPATIAL EXPRESSION CASCADES AND ASSEMBLY ON A CHIP

DNA brushes could be utilized to realize spatially resolved expression cascades as a step toward information transfer and expression patterns on a chip. To that end we have been using a cell-free transcription-translation extract to express proteins from DNA brushes. The first attempt included a two-stage cascade circuit realized on a chip by using two DNA constructs patterned in different neighboring stripe brushes: one encoding the T7 RNAP gene under the control of SP6 promoter, and the

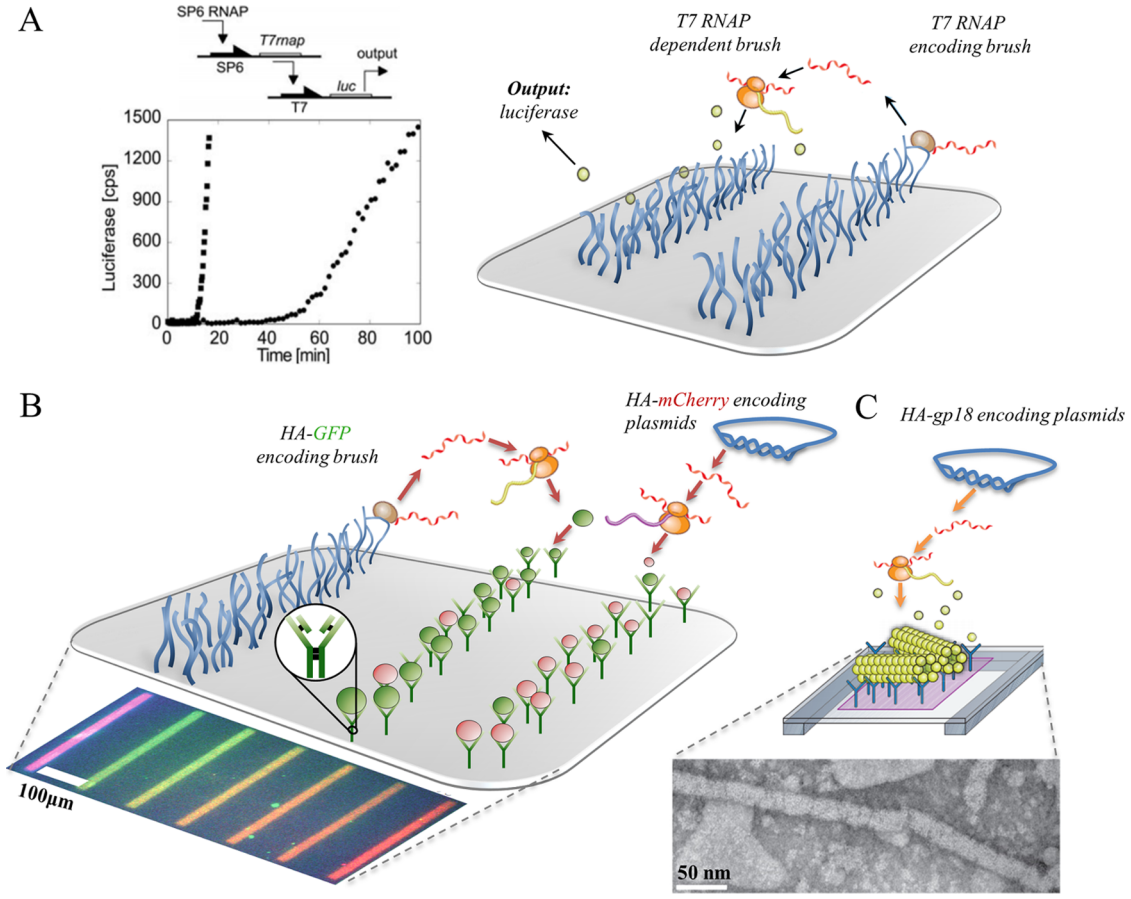

Figure 5. Cell-free spatial expression cascades and protein assembly on a chip. (A) Kinetics of luciferase expression as measured by luminescence in a two-gene cascade realized in spatially resolved brushes encoding T7 RNAP under control of Sp6 promoter and luciferase under control of T7 promoter (scheme). Addition of SP6 RNAP (brown) initiates the cascade, followed by protein translation by ribosomes (orange) resulting in a 60 min delayed expression of luciferase (yellow) compared to a single-step luciferase expression with only a 15 min delay. Reproduced with permission from ref 42. Copyright 2007 WILEY VCH. (B) Parallel synthesis of HA-mCherry (red) from plasmid DNA in solution and HA-GFP (green) from surface-bound DNA (blue) generates opposite gradients of GFP and mCherry bound to antibody traps on the surface (Y shapes), as seen by overlaying the red and green fluorescent channels. Reproduced with permission from ref 31. Copyright 2012 Nature Publishing Group. (C) In situ synthesis of T4 phage gp18 protein (yellow) from a plasmid in solution in the presence of antibody traps which serve as nucleation sites for growth of gp18 nanotubes on the surface. Reproduced with permission from ref 31. Copyright 2012 Nature Publishing Group.

other encoding *luciferase* under control of T7 promoter.[42] The SP6 RNAP was the input to initiate transcription/translation of T7 RNAP, which in turn cascaded to delay luciferase expression (Figure 5A).

In another example, an on/off switch controlling spatially resolved expression of GFP was demonstrated by assembling two DNA brushes: one coding for GFP but lacking the promoter sequence essential for its expression, and the other including promoter but no coding sequence. Enzymatic DNA cleavage and ligation on the surface resulted in DNA shuffling between brushes. After washing, the merging of promoters with GFP coding sequences was proven by the addition of cell-free extract, resulting in expression of GFP from the newly ligated brush.[49]

Recent experiments showed a new class of cascades with expression and trapping of proteins on the surface. This was done using a brush coding for GFP fused to the high-affinity HA peptide tag patterned next to anti HA-specific antibodies.[31] The experiment was extended to create a spatial genotype–phenotype linkage at the micrometer scale in which synthesized GFP gets trapped only close to its encoding brush. An additional protein was synthesized from a plasmid in bulk solution, HA-mCherry, which competed with HA-GFP for the same antibody traps. The resulting pattern was a surface gradient of trapped GFP whose density decreased with the distance from the brush, along with an inverted gradient of mCherry (Figure 5B).

Proteins synthesized in cell-free reactions maintain their ability to self-assemble into structural complexes. In the presence of liposomes, in vitro transcription–translation of nine proteins of *E. coli* ATP synthase resulted in assembly of a structural complex resembling the in vivo purified structure.[27] The five subunits of the *E. coli* RNA polymerase expressed in a semisynthetic cell-free PURE system,[72] assembled to form a functional enzyme capable of completing a full transcription cycle.[26] Remarkably, by supplementing a cell-free reaction with merely the genome of T7 bacteriophage, mature viral particles capable of infection were produced.[30] Assembly in cell-free expression reactions is decoupled from its natural setting and may, therefore, be rewired to produce novel structures and functions. As a model system for programmable design, T4 bacteriophage gp18 proteins were synthesized and assembled in a cell-free bulk reaction into micrometer long protein tubes, much longer than its 100 nm fixed length within the T4

dx.doi.org/10.1021/ar5001428 | *Acc. Chem. Res.* 2014, 47, 1912–1921

bacteriophage particle.[29] Coexpression of gp18 with gp15, another T4 protein, resulted in the sporadic closure of gp18 nanotubes into doughnuts.[29]

Could anchoring of proteins onto antibody traps serve as a scaffold for programmable macromolecular assembly? We addressed this question by adapting the biochip to combine surface patterning with transmission electron microscopy imaging on 8 nm thin glass support grids.[31] When HA-gp18 tubes were expressed and assembled in a solution cell-free reaction and subsequently added to anti-HA antibodies patterned on the chip, almost no tubes could be imaged on the traps. In contrast, when HA-gp18 expression occurred in a cell-free reaction bathing surface-patterned antibody traps, nanotubes were enriched at the patterned regions but to a much lesser extent elsewhere (Figure 5C). As preassembled nanotubes fail to bind the traps, most likely due to steric hindrance of HA tag at the assembled conformation, antibody traps seem to serve as nucleation sites for growth of nanotubes when their assembly is coupled to synthesis in the presence of traps.[31]

■ OUTLOOK

We envision DNA brushes as genomes of synthetic cell modules and, as such, characterized their biophysical and biochemical properties. By analogy to DNA in the cell, the expression machinery interacting with the brush responds to its density, conformation, and organization. Unlike DNA in a cell, many parameters of DNA brushes, such as height, density, composition, and orientation, can be simply altered. Whether the emergent properties of DNA brushes teach us something about gene expression in vivo might be arguable, yet they provide design tools for artificial biosystems. For example, it would be interesting to use coexisting phases of condensed and uncondensed brushes to spatially regulate gene expression.

One of the major advantages of the DNA brush is its coding capacity with thousands of genes assembled in a small volume. This high local gene concentration, in principle, enables expression of thousands of proteins in cell-free extracts. However, the observed protein exclusion from a DNA brush currently sets an upper limit on its expression capacity. Further research could explore conditions to counteract this exclusion by macromolecular crowding. We speculate that addition of inert macromolecules to the surrounding solution of the brush at cellular concentrations may cancel out entropy-driven exclusion and might induce confinement of RNAP due to its high affinity to DNA. Transcription rates are in turn expected to increase and surpass those in dilute solutions, possibly revealing an unexplored regime of biochemical activity.

Localized DNA brushes on a chip expressing proteins under regulation of gene circuits could lead to spatiotemporal patterns at the scale of an embryo, similarly to those obtained in a macroscopic gel,[8] and to biomolecular reaction-diffusion waves.[24,72] Such systems would open new means to study general principles of gene expression dynamics and information processing at the scale and conditions approaching a cell. Cell extracts based on *E. coli*'s endogenous transcription/translation and degradation machinery provide a toolbox for circuit design based on natural or synthetic regulatory elements,[12,73] which would lead to emergent expression patterns. Spatial gradients require source-sink dynamics that have so far been difficult to obtain with current protein degradation capacity.[74] Protein degradation in cell-free expression systems must be boosted to achieve effective turnover, or alternative mechanisms for turnover must be sought.

The combination of DNA brushes and surface traps for proteins and nucleic acids could be used to reconstitute multigene pathways, such as those governing T4 assembly.[41] Geometric layouts on the chip could be used to govern which genes are expressed, in which order, and where the proteins assemble into multicomponent structures. Fluorescence imaging, along with structural information obtained by electron and atomic force microscopy, following on-chip expression and assembly, may ultimately allow us to design novel functional protein and nuclei acid machines.

■ AUTHOR INFORMATION

Notes

The authors declare no competing financial interest.

Biographies

Dan Bracha attained his Ph.D. in 2013 at WIS with R. H. Bar-Ziv.

Eyal Karzbrun is in his last year of Ph.D. studies at WIS with R. H. Bar-Ziv.

Shirley S. Daube is a staff scientist at WIS.

Roy H. Bar-Ziv is a group leader at WIS.

■ ACKNOWLEDGMENTS

The authors wish to acknowledge the contribution of former lab members Amnon Buxboim, Maya Bar-Dagan, Yael Heyman, Maya Bar, Yahel Atsmon, and Gabriel Shemer. E.K. thanks the Azrieli Foundation for the Azrieli Fellowship. This work was supported by the Israel Science Foundation, the Minerva Foundation, the US−Israel Binational Foundation, and the Volkswagen foundation.

■ REFERENCES

(1) Fulton, A. B. How Crowded Is the Cytoplasm? *Cell* **1982**, *30*, 345−347.
(2) Zimmerman, S. B.; Trach, S. O. Estimation of Macromolecule Concentrations and Excluded Volume Effects for the Cytoplasm of Escherichia Coli. *J. Mol. Biol.* **1991**, *222*, 599−620.
(3) Turing, A. The Chemical Basis of Morphogenesis. *Philos. Trans. R. Soc. London* **1952**, *237*, 37−72.
(4) Nüsslein-Volhard, C.; Wieschaus, E. Mutations Affecting Segment Number and Polarity in Drosophila. *Nature* **1980**, *287*, 795−801.
(5) Mizushima, S.; Nomura, M. Assembly Mapping of 30S Ribosomal Proteins from *E. coli*. *Nature* **1970**, *226*, 1214−1218.
(6) Edgar, R. S.; Wood, W. B. Morphogenesis of Bacteriophage T4 in Extracts of Mutant-Infected Cells. *Proc. Natl. Acad. Sci. U.S.A.* **1966**, *55*, 498−505.
(7) Noireaux, V.; Bar-Ziv, R.; Libchaber, A. Principles of Cell-Free Genetic Circuit Assembly. *Proc. Natl. Acad. Sci. U.S.A.* **2003**, *100*, 12672−12677.
(8) Isalan, M.; Lemerle, C.; Serrano, L. Engineering Gene Networks to Emulate Drosophila Embryonic Pattern Formation. *PLoS Biol.* **2005**, *3*, e64.
(9) Kim, J.; White, K. S.; Winfree, E. Construction of an in Vitro Bistable Circuit from Synthetic Transcriptional Switches. *Mol. Syst. Biol.* **2006**, *2*, 68.
(10) Kim, J.; Winfree, E. Synthetic in Vitro Transcriptional Oscillators. *Mol. Syst. Biol.* **2011**, *7*, 465.
(11) Franco, E.; Friedrichs, E.; Kim, J.; Jungmann, R.; Murray, R.; Winfree, E.; Simmel, F. C. Timing Molecular Motion and Production with a Synthetic Transcriptional Clock. *Proc. Natl. Acad. Sci. U.S.A.* **2011**, *108*, E784−793.

(12) Shin, J.; Noireaux, V.; An, E. Coli Cell-Free Expression Toolbox: Application to Synthetic Gene Circuits and Artificial Cells. *ACS Synth. Biol.* **2012**, *1*, 29−41.
(13) Niederholtmeyer, H.; Stepanova, V.; Maerkl, S. J. Implementation of Cell-Free Biological Networks at Steady State. *Proc. Natl. Acad. Sci. U.S.A.* **2013**, *110*, 15985−15990.
(14) Sun, Z. Z.; Yeung, E.; Hayes, C. A.; Noireaux, V.; Murray, R. M. Linear DNA for Rapid Prototyping of Synthetic Biological Circuits in an *Escherichia coli* Based TX-TL Cell-Free System. *ACS Synth. Biol.* **2013**, DOI: 10.1021/sb400131a.
(15) Tawfik, D. S.; Griffiths, A. D. Man-Made Cell-like Compartments for Molecular Evolution. *Nat. Biotechnol.* **1998**, *16*, 652−656.
(16) Noireaux, V.; Libchaber, A. A Vesicle Bioreactor as a Step toward an Artificial Cell Assembly. *Proc. Natl. Acad. Sci. U.S.A.* **2004**, *101*, 17669−17674.
(17) Ishikawa, K.; Sato, K.; Shima, Y.; Urabe, I.; Yomo, T. Expression of a Cascading Genetic Network within Liposomes. *FEBS Lett.* **2004**, *576*, 387−390.
(18) Maeda, Y. T.; Nakadai, T.; Shin, J.; Uryu, K.; Noireaux, V.; Libchaber, A. Assembly of MreB Filaments on Liposome Membranes: A Synthetic Biology Approach. *ACS Synth. Biol.* **2012**, *1*, 53−59.
(19) Saeki, D.; Sugiura, S.; Kanamori, T.; Sato, S.; Ichikawa, S. Microcompartmentalized Cell-Free Protein Synthesis in Semipermeable Microcapsules Composed of Polyethylenimine-Coated Alginate. *J. Biosci. Bioeng.* **2014**, DOI: 10.1016/j.jbiosc.2014.01.014.
(20) Sokolova, E.; Spruijt, E.; Hansen, M. M. K.; Dubuc, E.; Groen, J.; Chokkalingam, V.; Piruska, A.; Heus, H. a; Huck, W. T. S. Enhanced Transcription Rates in Membrane-Free Protocells Formed by Coacervation of Cell Lysate. *Proc. Natl. Acad. Sci. U.S.A.* **2013**, *110*, 11692−11697.
(21) Weitz, M.; Kim, J.; Kapsner, K.; Winfree, E.; Franco, E.; Simmel, F. C. Diversity in the Dynamical Behaviour of a Compartmentalized Programmable Biochemical Oscillator. *Nat. Chem.* **2014**, *6*, 295−302.
(22) Seelig, G.; Soloveichik, D.; Zhang, D. Y.; Winfree, E. Enzyme-Free Nucleic Acid Logic Circuits. *Science* **2006**, *314*, 1585−1588.
(23) Zhang, D. Y.; Turberfield, A. J.; Yurke, B.; Winfree, E. Engineering Entropy-Driven Reactions and Networks Catalyzed by DNA. *Science* **2007**, *318*, 1121−1125.
(24) Padirac, A.; Fujii, T.; Estévez-Torres, A.; Rondelez, Y. Spatial Waves in Synthetic Biochemical Networks. *J. Am. Chem. Soc.* **2013**, *135*, 14586−14592.
(25) Qian, L.; Winfree, E.; Bruck, J. Neural Network Computation with DNA Strand Displacement Cascades. *Nature* **2011**, *475*, 368−372.
(26) Asahara, H.; Chong, S. In Vitro Genetic Reconstruction of Bacterial Transcription Initiation by Coupled Synthesis and Detection of RNA Polymerase Holoenzyme. *Nucleic Acids Res.* **2010**, *38*, e141.
(27) Matthies, D.; Haberstock, S.; Joos, F.; Dötsch, V.; Vonck, J.; Bernhard, F.; Meier, T. Cell-Free Expression and Assembly of ATP Synthase. *J. Mol. Biol.* **2011**, *413*, 593−603.
(28) Jewett, M. C.; Fritz, B. R.; Timmerman, L. E.; Church, G. M. In Vitro Integration of Ribosomal RNA Synthesis, Ribosome Assembly, and Translation. *Mol. Syst. Biol.* **2013**, *9*, 678.
(29) Daube, S. S.; Arad, T.; Bar-Ziv, R. Cell-Free Co-Synthesis of Protein Nanoassemblies: Tubes, Rings, and Doughnuts. *Nano Lett.* **2007**, *7*, 638−641.
(30) Shin, J.; Jardine, P.; Noireaux, V. Genome Replication, Synthesis, and Assembly of the Bacteriophage T7 in a Single Cell-Free Reaction. *ACS Synth. Biol.* **2012**, *1*, 408−413.
(31) Heyman, Y.; Buxboim, A.; Wolf, S. G.; Daube, S. S.; Bar-Ziv, R. H. Cell-Free Protein Synthesis and Assembly on a Biochip. *Nat. Nanotechnol.* **2012**, *7*, 374−378.
(32) Padirac, A.; Fujii, T.; Rondelez, Y. Bottom-up Construction of in Vitro Switchable Memories. *Proc. Natl. Acad. Sci. U.S.A.* **2012**, *109*, E3212−20.
(33) Szostak, J. W.; Bartel, D. P.; Luisi, P. L. Synthesizing Life. *Nature* **2001**, *409*, 387−390.
(34) Forster, A. C.; Church, G. M. Towards Synthesis of a Minimal Cell. *Mol. Syst. Biol.* **2006**, *2*, 45.
(35) Luisi, P. L.; Ferri, F.; Stano, P. Approaches to Semi-Synthetic Minimal Cells: A Review. *Naturwissenschaften* **2006**, *93*, 1−13.
(36) Noireaux, V.; Maeda, Y. T.; Libchaber, A. Development of an Artificial Cell, from Self-Organization to Computation and Self-Reproduction. *Proc. Natl. Acad. Sci. U.S.A.* **2011**, *108*, 3473−3480.
(37) Hodgman, C. E.; Jewett, M. C. Cell-Free Synthetic Biology: Thinking Outside the Cell. *Metab. Eng.* **2012**, *14*, 261−269.
(38) Swartz, J. R. Transforming Biochemical Engineering with Cell-Free Biology. *AIChE J.* **2012**, *58*, 5−13.
(39) Hockenberry, A. J.; Jewett, M. C. Synthetic in Vitro Circuits. *Curr. Opin. Chem. Biol.* **2012**, *16*, 253−259.
(40) Genot, A. J.; Fujii, T.; Rondelez, Y. In Vitro Regulatory Models for Systems Biology. *Biotechnol. Adv.* **2013**, *31*, 789−796.
(41) Daube, S. S.; Bar-Ziv, R. H. Protein Nanomachines Assembly Modes: Cell-Free Expression and Biochip Perspectives. *Wiley Interdiscip. Rev. Nanomed. Nanobiotechnol.* **2013**, *5*, 613−628.
(42) Buxboim, A.; Bar-Dagan, M.; Frydman, V.; Zbaida, D.; Morpurgo, M.; Bar-Ziv, R. A Single-Step Photolithographic Interface for Cell-Free Gene Expression and Active Biochips. *Small* **2007**, *3*, 500−510.
(43) Buxboim, A.; Daube, S. S.; Bar-Ziv, R. Ultradense Synthetic Gene Brushes on a Chip. *Nano Lett.* **2009**, *9*, 909−913.
(44) Shemer, G.; Atsmon, Y.; Karzbrun, E.; Bar-Ziv, R. H. Collective Conformations of DNA Polymers Assembled on Surface Density Gradients. *J. Am. Chem. Soc.* **2012**, *134*, 3954−3956.
(45) Bracha, D.; Karzbrun, E. Entropy-Driven Collective Interactions in DNA Brushes on a Biochip. *Proc. Natl. Acad. Sci. U.S.A.* **2013**, *110*, 4534−4538.
(46) Bracha, D.; Bar-Ziv, R. Dendritic and Nanowire Assemblies of Condensed DNA Polymer Brushes. *J. Am. Chem. Soc.* **2014**, *136*, 4945−4953.
(47) Buxboim, A.; Daube, S. S.; Bar-Ziv, R. Synthetic Gene Brushes: A Structure-Function Relationship. *Mol. Syst. Biol.* **2008**, *4*, 181.
(48) Daube, S. S.; Bracha, D.; Buxboim, A.; Bar-Ziv, R. H. Compartmentalization by Directional Gene Expression. *Proc. Natl. Acad. Sci. U.S.A.* **2010**, *107*, 2836−2841.
(49) Bar, M.; Bar-Ziv, R. H. Spatially Resolved DNA Brushes on a Chip: Gene Activation by Enzymatic Cascade. *Nano Lett.* **2009**, *9*, 4462−4466.
(50) Pincus, P. Colloid Stabilization with Grafted Polyelectrolytes. *Macromolecules* **1991**, *24*, 2912−2919.
(51) Halperin, A.; Tirrell, M.; Lodge, T. Tethered Chains in Polymer Microstructures. *Macromol. Synth. Order Adv. Prop.* **1992**, 100.
(52) Israels, R.; Leermakers, F. a. M.; Fleer, G. J.; Zhulina, E. B. Charged Polymeric Brushes: Structure and Scaling Relations. *Macromolecules* **1994**, *27*, 3249−3261.
(53) Kegler, K.; Konieczny, M.; Dominguez-Espinosa, G.; Gutsche, C.; Salomo, M.; Kremer, F.; Likos, C. N. Polyelectrolyte-Compression Forces between Spherical DNA Brushes. *Phys. Rev. Lett.* **2008**, *100*, 1−4.
(54) Benoit, H.; Doty, P. Light Scattering from Non-Gaussian Chains. *J. Phys. Chem.* **1953**, *57*, 958−963.
(55) Nepal, M.; Yaniv, A.; Shafran, E.; Krichevsky, O. Structure of DNA Coils in Dilute and Semidilute Solutions. *Phys. Rev. Lett.* **2013**, *110*, 058102.
(56) Alexander, S. Polymer Adsorption on Small Spheres. A Scaling Approach. *J. Phys. (Paris)* **1977**, *38*, 977−981.
(57) Gosule, L.; Schellman, J. Compact Form of DNA Induced by Spermidine. *Nature* **1976**, *259*, 333−335.
(58) Pelta, J.; Durand, D.; Doucet, J.; Livolant, F. DNA Mesophases Induced by Spermidine: Structural Properties and Biological Implications. *Biophys. J.* **1996**, *71*, 48−63.
(59) Bloomfield, V. A. DNA Condensation. *Curr. Opin. Struct. Biol.* **1996**, *6*, 334−341.
(60) Livolant, F. Ordered Phases of DNA in Vivo and in Vitro. *Phys. A (Amsterdam, Neth.)* **1991**, *176*, 117−137.
(61) Teif, V. B.; Bohinc, K. Condensed DNA: Condensing the Concepts. *Prog. Biophys. Mol. Biol.* **2011**, *105*, 208−222.

(62) Ubbink, J.; Odijk, T. Deformation of Toroidal DNA Condensates under Surface Stress. *Eur. Lett.* **1996**, *33*, 353−358.
(63) Bouligand, Y.; Norris, V. Chromosome Separation and Segregation in Dinoflagellates and Bacteria May Depend on Liquid Crystalline States. *Biochimie* **2001**, *83*, 187−192.
(64) Smeekens, S. P.; Romano, L. J. Promoter and Nonspecific DNA Binding by the T7 RNA Polymerase. *Nucleic Acids Res.* **1986**, *14*, 2811−2827.
(65) Sutherland, H.; Bickmore, W. A. Transcription Factories: Gene Expression in Unions? *Nat. Rev. Genet.* **2009**, *10*, 457−466.
(66) Lewis, P. J.; Thaker, S. D.; Errington, J. Compartmentalization of Transcription and Translation in Bacillus Subtilis. *EMBO J.* **2000**, *19*, 710−718.
(67) Zimmerman, S. B. Shape and Compaction of Escherichia Coli Nucleoids. *J. Struct. Biol.* **2006**, *156*, 255−261.
(68) Göndör, A.; Ohlsson, R. Chromosome Crosstalk in Three Dimensions. *Nature* **2009**, *461*, 212−217.
(69) Wang, X.; Montero Llopis, P.; Rudner, D. Z. Organization and Segregation of Bacterial Chromosomes. *Nat. Rev. Genet.* **2013**, *14*, 191−203.
(70) Le, T. B. K.; Imakaev, M. V.; Mirny, L. A.; Laub, M. T. High-Resolution Mapping of the Spatial Organization of a Bacterial Chromosome. *Science* **2013**, *342*, 731−734.
(71) Naumova, N.; Imakaev, M.; Fudenberg, G.; Zhan, Y.; Lajoie, B. R.; Mirny, L. A.; Dekker, J. Organization of the Mitotic Chromosome. *Science* **2013**, *342*, 948−953.
(72) Shimizu, Y.; Inoue, a; Tomari, Y.; Suzuki, T.; Yokogawa, T.; Nishikawa, K.; Ueda, T. Cell-Free Translation Reconstituted with Purified Components. *Nat. Biotechnol.* **2001**, *19*, 751−755.
(73) Shin, J.; Noireaux, V. Efficient Cell-Free Expression with the Endogenous *E. coli* RNA Polymerase and Sigma Factor 70. *J. Biol. Eng.* **2010**, *4*, 8.
(74) Karzbrun, E.; Shin, J.; Bar-Ziv, R. H.; Noireaux, V. Coarse-Grained Dynamics of Protein Synthesis in a Cell-Free System. *Phys. Rev. Lett.* **2011**, *106*, 048104.